

1  
2  
3  
4  
5  
6  
7  
8  
9  
10  
11  
12  
13  
14  
15  
16  
17  
18  
19  
20  
21  
22  
23  
24  
25  
26  
27  
28  
29

# The impact of tropical tropopause cooling on Sahelian extreme deep convection

**Kunihiko Kodera<sup>1</sup>**

*Meteorological Research Institute  
Tsukuba, 305-0052, Japan*

**Nawo Eguchi**

*Research Institute for Applied Mechanics  
Kyushu University, Kasuga, 816-8580, Japan*

**Rei Ueyama**

*NASA Ames Research Center, Moffett Field, 94035-0001, USA*

**Beatriz M. Funatsu**

*CNRS, Université de Nantes, UMR 6554 LETG, Campus du Tertre  
Nantes, 44312, France*

**Marco Gaetani**

*Universitaria Superiore IUSS, Pavia, 27100, Italy*

**and**

**Christopher M. Taylor**

*UK Centre for Ecology and Hydrology, Wallingford, OX10 8BB, UK  
National Centre for Earth Observation, Wallingford, OX10 8BB, UK*

24 April, 2021

1) Corresponding author: Kunihiko Kodera, Meteorological Research Institute, Tsukuba, JAPAN.

Email: [kodera.kk@gmail.com](mailto:kodera.kk@gmail.com)

## Abstract

30  
31 Previous studies have suggested that the recent increase in tropical extreme deep  
32 convection, in particular over Asia and Africa during the boreal summer, has occurred in  
33 association with a cooling in the tropical lower stratosphere. The present study is focused  
34 on the Sahel region of West Africa, where an increased occurrence of extreme precipitation  
35 events has been reported over recent decades. The results show that the changes over  
36 West Africa since the 1980s involve a cooling trend in the tropical lower stratosphere and  
37 tropopause layer, combined with a warming in the troposphere. This feature is similar to that  
38 which might result from increased greenhouse gas levels, but is distinct from the interannual  
39 variation of precipitation associated with the transport of water vapor from the Atlantic Ocean.  
40 It is suggested that the decrease in the vertical temperature gradient in the tropical  
41 tropopause region enhances extreme deep convection over the Sahel, where penetrating  
42 convection is frequent, whereas tropospheric warming suppresses the shallower convection  
43 over the Guinea Coast. The essential feature of the recent changes over West Africa is  
44 therefore the depth of convection, rather than the total amount of surface precipitation.

45  
46 **Keywords** Sahel; recent trend; tropical tropopause layer; deep convection; land  
47 precipitation;

## 49 1. Introduction

50 West Africa is particularly susceptible to the impacts of climate change, with rising  
51 temperatures already threatening human health (Russo et al., 2016) and significant changes  
52 in the precipitation regime likely to occur over the next few decades (Gaetani et al., 2020).  
53 Assessing the role of the tropical tropopause layer (TTL; around 140–70 hPa) in driving  
54 precipitation trends is a valuable step forward that will improve our understanding of the  
55 present and future evolution of the rainfall regime in West Africa.

56

57 Koderer et al. (2019) have indicated that extreme deep convection in the ascending branch  
58 of the boreal summer Hadley circulation became more active over recent decades,  
59 particularly over the African and Asian sectors. In West Africa, this increase in convective  
60 activity was associated with the recent recovery of rainfall over the Sahel following the long  
61 and severe drought conditions of the 1970s and 1980s (Fontaine et al., 2011; Nicholson,  
62 2013; Maidment et al., 2015). This recovery was linked to accelerating global warming,  
63 which increased moist static energy in the troposphere over West Africa by enhancing local  
64 evaporation (Giannini, 2010) and also strengthened moisture transport from the subtropical  
65 North Atlantic (Giannini et al., 2013; Dong and Sutton, 2015). The present increase in  
66 precipitation over the Sahel is, however, not a simple recovery to the former wet state: the  
67 characteristics of rainfall have also changed, becoming more intense and intermittent.  
68 According to Panthou et al. (2014, 2018) the number of rainy days per year is still below

69 average, implying that there has been an increase in severe rainfall events. It should be  
70 noted that the increase of rainfall has not occurred uniformly over West Africa; for example,  
71 rainfall decreased somewhat over the Guinea coastal region (Odoulami and Akinsanola,  
72 2017).

73

74 As hydrological changes have a major impact on human activity in West Africa (Sultan and  
75 Gaetani, 2016), a number of studies have investigated precipitation at the surface, as  
76 documented in review papers (Rodríguez-Fonseca et al., 2011; Biasutti, 2019). These  
77 studies have demonstrated the important role of sea surface temperatures (SSTs) with  
78 respect to the last drought over the Sahel (Folland et al.,1986; Mohino et al., 2011;  
79 Rodríguez-Fonseca et al., 2015). Interannual variation of rainfall is also related to the phase  
80 of El Niño–Southern Oscillation (ENSO; Janicot et al.,1996; Diakhaté et al., 2019; Hart et  
81 al., 2019). However, state-of-the-art climate models still struggle to reproduce precipitation  
82 variability and trends in West Africa through the historical period, which is mainly due to their  
83 low skill in simulating the observed SST teleconnections (Rowell, 2013).

84

85 Taylor et al. (2017; hereafter referred to as T17) showed that the occurrence frequency of  
86 mesoscale convective systems (MCSs) with a cloud top temperature (CTT) of less than  
87  $-70^{\circ}\text{C}$  has tripled since the mid-1980s, while more common MCSs with CCT up to  $-40^{\circ}\text{C}$   
88 have increased only moderately in frequency. They investigated the role of recent Saharan

89 warming, enhanced wind shear, and changes in the properties of the Saharan Air Layer as  
90 drivers of MCS intensification. Further evidence supporting the important role of enhanced  
91 meridional temperature gradients in deepening MCSs has subsequently been presented for  
92 the wider tropical North African region (Taylor et al., 2018; Klein and Taylor, 2020; Klein et  
93 al., 2020). The increase in the number of cold cloud top MCSs can be related to the increase  
94 in extreme rainfall events over the Sahel (Klein et al., 2018). Note that an air temperature of  
95  $-70^{\circ}\text{C}$  roughly corresponds to the 140-hPa level at the bottom of the TTL. This suggests the  
96 possible role of TTL processes in the recent precipitation increase over the Sahel. In the  
97 present study, we will demonstrate the importance of TTL processes for explaining this  
98 rainfall recovery and show that the atmospheric circulation associated with the precipitation  
99 increase is somewhat different from the accepted paradigm based on the transport of water  
100 vapor from the ocean (Druyan and Koster, 1989; Pu and Cook, 2011; Giannini et al., 2013).

101

## 102 **2. Data**

103 We make use of monthly mean meteorological reanalysis data by the Japan Meteorological  
104 Agency, JRA-55 (Kobayashi et al., 2015), during the period of satellite observation era after  
105 1979. For this study, we defined the climatology as the 40-year mean for the period 1979–  
106 2018 (unless stated otherwise), and the standard deviation was also calculated over this  
107 period.

108

109 Analysis of the surface precipitation was performed using Global Precipitation Climatology  
110 Project (GPCP) monthly mean data version 2.3 (Adler et al., 2003). Extreme deep  
111 convection, such as tropical overshooting clouds (COV) that penetrate beyond the level of  
112 neutral buoyancy and overshoot into the TTL, were identified using the diagnostics  
113 developed by Hong et al. (2005). These diagnostics are based on brightness temperature  
114 differences measured by three high-frequency channels of the Advanced Microwave  
115 Sensing Unit (AMSU) or the Microwave Humidity Sensor (MHS) for the period 2001 to 2018  
116 (Funatsu et al., 2016), and this is similar to the approach used by Kodera et al. (2019). We  
117 compared our results with the occurrence frequency of MCSs over the Sahel obtained by  
118 T17.

119

### 120 **3. Results**

121 The changes in precipitation during the summer monsoon season of July, August, and  
122 September (JAS), from the 1980s to the present have not occurred homogeneously over  
123 West Africa (Fig. 1). Precipitation increased over the Sahel (15°W–20°E, 12.5°N–17.5°N;  
124 Fig. 1c), but decreased over the Guinea Coast (15°W–20°E, 2.5°N–7.5°N; Fig. 1d), as also  
125 reported by Odoulami and Akinsanola (2017). In fact, the surface precipitation does not  
126 show a clear trend when averaged over the whole of West Africa (15°W–20°E, 2.5°N–  
127 17.5°N; (Fig. 1e).

128

Fig. 1

129 In fact, convective activity varies strongly within West Africa during the monsoon season;  
130 e.g., broad stratiform clouds occur frequently over the coastal region, whereas extreme deep  
131 convection is common further inland (Zuluaga and Houze, 2015). A decreasing precipitation  
132 trend is particularly pronounced over the coastal regions west of the Guinea Highlands and  
133 South Cameroon Plateau (Fig. 1b). Over these elevated terrains, convergence of the air  
134 from the ocean (Fig. 2c) results in heavy precipitation (Fig. 1a). As the convection over the  
135 coastal region is generally not deep enough to penetrate into the TTL, uplifted air diverges  
136 in the upper troposphere (Fig. 2b). An increasing precipitation trend is found in regions of  
137 high equivalent potential temperature near the surface (Fig. 2e), where extreme deep  
138 convective clouds with overshooting tops occur (Fig. 2d). This extreme deep convection is  
139 also evident in the large horizontal divergence at higher levels in the TTL (Fig. 2a).

Fig. 2

140  
141 These results suggest that the regional differences in recent precipitation trends (Fig. 1b)  
142 may arise from difference in the structure of convection. In particular, precipitation increased  
143 where extreme deep convection occurs frequently, but decreased where convection is  
144 relatively shallow. This implies the important role of the depth of convection in precipitation  
145 changes over the last few decades.

146  
147 We will now focus on the Sahelian region. The time series shown in Fig. 1c is also shown in  
148 Fig. 3a. Large interannual variations are superimposed over the increasing precipitation

Fig. 3

149 trend. The red dots and black crosses denote the maxima and minima, respectively, in the  
150 interannual variations. The first thing to clarify is whether the decadal trend is produced by  
151 the same processes that cause the year-to-year variability. To investigate this, we carried  
152 out composite analysis of the standardized anomalies; i.e., anomalies normalized using the  
153 standard deviation of the interannual variation. For the composite means of the year-to-year  
154 variation, the 8 largest positive deviations in precipitation above the linear trend line (wet  
155 years: 1980, 1986, 1988, 1994, 1999, 2003, 2010, 2012) and the same number of  
156 precipitation minima below the linear trend line (dry years: 1984, 1987, 1990, 1997, 2002,  
157 2004, 2011, and 2014) were selected.

158

159 Composite differences between dry and wet years are indicated in the left-hand panels of  
160 Fig. 3, and the composite differences between two 19-year periods, 2000–2018 and 1979–  
161 1997, are shown in the right-hand panels. Naturally, we see an increase in the precipitation  
162 over the Sahel in both cases, although the contrast between increased precipitation in the  
163 Sahel and decreased precipitation over the Guinea Coast is more pronounced in the decadal  
164 changes (Fig. 3e). The relationship between moisture flux and precipitation over Africa has  
165 been investigated. Large differences in environmental conditions are seen from the zonal  
166 moisture flux in the lower troposphere (Fig. 3c). The anomalous zonal moisture flux at 850  
167 hPa extends from the Atlantic Ocean over the African continent during wet years. This  
168 feature is consistent with the feedback process proposed by Rowell (2003), whereby



169 precipitation increases over the Sahel due to a teleconnection from remote oceans, which  
170 induces stronger westerlies over the Atlantic Ocean, thus transporting more water vapor  
171 over the continent and further increasing precipitation over the Sahel. The decadal changes,  
172 however, indicate a weaker connection to the moisture flux from the oceanic sector (Fig. 3f).  
173 Occurrence of wet and dry years correspond well to years of large and small eastward  
174 moisture flux, respectively, driven by zonal wind over the Atlantic Ocean (Fig. 7c). Decadal  
175 change of water vapor flux rather shows a meridional seesaw between Sahel and Guinea  
176 Coast. Thus, the overall change in Western Africa is small, consistent with the insignificant  
177 trend in precipitation averaged over the Western Africa (Fig. 1e). We note that some of the  
178 wet years (1988, 1999, 2010) correspond to La Niña years, while some of the dry years  
179 (1987, 1997, 2002) correspond to El Niño years. This suggests a possible role of ENSO  
180 variability in influencing the decadal trend. However, Pomposi et al. (2020) found minor  
181 influence of ENSO variability in the recent precipitation trend in West Africa.

182

183 Increased precipitation induces upwelling in the atmosphere. The year-to-year variability  
184 suggests that this response is limited mainly in the troposphere (Fig. 3d). However, the  
185 decadal changes indicate that upwelling generally increased in the TTL, except for a region  
186 of suppressed tropospheric upwelling over the West African coast. In the following, we  
187 investigate why the decadal changes in pressure vertical velocity ( $\omega$ ) differ between the  
188 Sahel and the Guinea Coast.

189

190 The evolution of the JAS mean anomalous temperature (T) and pressure vertical velocity  
191 over West Africa is illustrated in Fig. 4. The amplitude of vertical velocity is shown relative to  
192 the climatological value,  $\omega_{\text{clim}}$ , as  $(\omega/\omega_{\text{clim}}) \times 100$ . Black and red contours indicate ratios  
193 greater or less than 100%, respectively. Although there is no clear trend in the surface  
194 precipitation averaged over West Africa (Fig. 1e), trends are evident in the temperature and  
195 vertical velocity in the TTL. In particular, the temperature decreased by more than 2 K over  
196 this time period, while the vertical velocity increased four-fold from 50% to 200% around  
197 150– 100 hPa. A decreasing trend in the upwelling in the troposphere is also seen in  
198 association with the tropospheric warming trend.

Fig. 4

199

200 The evolution of the temperature and horizontal divergence are shown in Fig. 5a and 5b for  
201 the Sahel and Guinea Coast separately. The vertical velocity in both regions is shown in Fig.  
202 5c and 5d. Cooling trends in the lower stratosphere and TTL are found in both regions. The  
203 divergence field indicates that convection over the Sahel reaches the TTL. It should be noted  
204 that a cooling in the TTL can enhance deep convective activity, consistent with that found in  
205 a study on a sudden stratospheric warming (SSW) in January (Eguchi et al., 2015). In  
206 contrast, because convection over the Guinea Coast is not very deep, downwelling persists  
207 in the upper troposphere between 200-150 hPa. This indicates a clear separation between  
208 the upwelling in the stratosphere and troposphere. Accordingly, although cooling and

Fig. 5

209 upwelling trends are found in both the lower stratosphere and TTL, tropospheric vertical  
210 velocity does not show an increasing trend over the Guinea Coast.

211

212 Latitudinal differences between the two regions can clearly be seen in the meridional cross-  
213 section of JAS mean standardized temperature and vertical velocity anomalies shown in Fig.  
214 6. Although cooling in the TTL occurred over a range of latitudes, upwelling in the  
215 troposphere was enhanced over the Sahel, but suppressed over the Guinea Coast. The  
216 widespread cooling over regions of both increasing and decreasing convection suggests  
217 that lower stratospheric temperatures are driving the changes in convection and not a simple  
218 response to convective activity (Holloway and Neelin 2007). This leads to a working  
219 hypothesis that the cooling in the TTL impacts mainly those regions where upwelling extends  
220 from the upper troposphere to the TTL (*i.e.*, about 200 to 140 hPa), as indicated by the  
221 climatological divergence field (dotted lines).

222

223 Figures 6b and 6c show the evolution of standardized COV frequencies during the period  
224 2001–2018. The mean occurrence frequency of COV over the Sahel is 4.4 ‰ which is four  
225 times as large as that over the Guinea Coast. There is an increasing trend superimposed  
226 on the year-to-year variability in the COV occurrence frequency over the Sahel, which  
227 matches the evolution of MCSs with a CTT of less than  $-70^{\circ}\text{C}$  reported by T17. In fact, the  
228 increase in MCSs over the Sahel had already begun in the 1980s, as will be shown in Fig.

Fig. 6

229 7. In contrast, the COV occurrence frequency over the Guinea Coast exhibits a decreasing  
230 trend.

231

232 We also compared the time series of the horizontal divergence at 125 hPa over the Sahel  
233 with the occurrence frequency of MCSs with a CTT below  $-70^{\circ}\text{C}$  obtained by T17. Note that  
234 the climatological air temperature around 125 hPa is about  $-75^{\circ}\text{C}$ . As expected, not only is  
235 the large increasing trend common to both properties, some in-phase interannual variability  
236 is also seen, with the correlation coefficient ( $r$ ) between the two being 0.87. Correlation  
237 coefficient between detrended time series of divergence and MCS is 0.47 and is still  
238 statistically significant for 35-year data (Fig. S1). It is noted, however, that the good  
239 correlation comes from the late period, when very cold MCSs became more frequent. It  
240 should also be noted that the vertical temperature gradient in the TTL (i.e., the temperature  
241 difference between 125 and 175 hPa) shows a decreasing trend, i.e. destabilization.

242

243 In the case of the divergence at the top of the troposphere at 200 hPa, we found a good  
244 correlation ( $r = 0.78$ ) between MCSs with a CTT below  $-40^{\circ}\text{C}$  (Fig. 7b). It was noted in T17  
245 that precipitation over the Sahel is better correlated with the more common MCSs (CTT <  
246  $-40^{\circ}\text{C}$ ;  $r = 0.88$ ) than the extremely cold MCSs. Increasing trends at the top of the  
247 troposphere are less pronounced than those in the TTL due to the large interannual  
248 variability, especially prior to 2000. Peaks in the year-to-year variability of horizontal

Fig. 7

249 divergence become more prominent at lower level. The divergence at 250 hPa correlates  
250 well ( $r = 0.77$ ) with the near-surface zonal wind velocity over the Atlantic Ocean west of  
251 Africa ( $10^{\circ}\text{N}$ – $15^{\circ}\text{N}$ ,  $30^{\circ}\text{W}$ – $15^{\circ}\text{W}$ ) (Fig. 7c). This is consistent with the analysis in Fig. 3d that  
252 the variation of the moisture flux from the ocean produces large year-to-year variability in  
253 the upwelling within the troposphere.

254

255 Seasonal differences in the spatial structure of temperature and vertical velocity in the West  
256 African sector are shown in Fig. 8. West African monsoon evolves during the summer: the  
257 landing of the rain belt on the coast occurs in May–June, and the actual Sahelian rain season  
258 occurs in July–September. The recent decadal change in temperature field shows very  
259 similar feature throughout the early and late summer with cooling in the stratosphere and  
260 warming in the troposphere (Figs. 8a and 8c), although the active center of the convection  
261 shifts northward in mid-summer from coastal region to over the continent (contours in Figs.  
262 8b and 8d). This suggests that the change in the temperature in the lower stratosphere does  
263 not reflect local convective activity.

264

265 Recent decadal changes in the vertical velocity in early summer (May–June) resulted in a  
266 suppression of upwelling in the troposphere in association with the warming there, but  
267 upwelling in the TTL enhanced in association with a cooling in the TTL and lower  
268 stratosphere. An increasing trend in the upwelling is also evident near the surface around

Fig. 8

269 the southern edge of the Sahara Desert, and this is associated with a large warming near  
270 the surface. The active center of convection shifts northward over land according to the  
271 seasonal march in mid-summer (July–August) (Fig. 8c and 8d). Deep convection in mid-  
272 summer becomes deeper and shifts northward in recent decades.

273

#### 274 **4. Discussion and Conclusions**

275 Recent precipitation trends in West Africa during the summer monsoon season differ  
276 according to the regional characteristics of convective activity. There is an increasing  
277 precipitation trend over the Sahel where extreme deep convection develops, whereas a  
278 decreasing precipitation trend is evident over the Guinea Coast where convection is  
279 relatively shallow (Figs 1 and 2). These trends support the findings of previous studies  
280 (Odoulami and Akinsanola, 2017; Biasutti, 2019). However, surface precipitation averaged  
281 over the entire West African region shows no clear trend (Fig. 1e), which suggests that the  
282 change in the total amount of water vapor transported over West Africa may not be essential  
283 for the recent decadal changes.

284

285 The different precipitation trends seen over the Sahel and Guinea Coast can be interpreted  
286 as a result of the differences in the depth of convective clouds in the two regions. Penetrating  
287 deep convection over the Sahel is susceptible to temperature changes in the TTL and thus  
288 increases in response to TTL cooling. In contrast, convective activity over the Guinea Coast

289 is not influenced by cooling in the TTL, but rather suppressed by warming in the troposphere.  
290

291 Although an increasing decadal trend in summer precipitation exists over the Sahel, there  
292 is also substantial year-to-year variability, which may be driven by the transport of water  
293 vapor from the Atlantic Ocean (Fig. 3). Modulation of the upward velocity by this year-to-  
294 year variability in precipitation is limited to the troposphere. In contrast, circulation changes  
295 related to the recent decadal trends are observed in the TTL. This suggests that the recent  
296 trends in circulation are driven by processes other than those producing the year-to-year  
297 variability in the tropospheric circulation.

298

299 Variations in the lower stratospheric temperature are similar between the Sahel and Guinea  
300 Coast regions (Fig. 5). However, in the Sahel, upwelling produced by convection is  
301 connected to the lower stratospheric circulation, whereas over the Guinea Coast,  
302 tropospheric upwelling is decoupled from the stratosphere. In the present analysis, we  
303 assumed that the horizontal divergence in the upper troposphere and TTL is related to  
304 detrained air around the cloud top in deep convection. This relationship was verified through  
305 a comparison of the horizontal divergence with the occurrence frequency of MCSs (Fig. 7).  
306

307 Panthou et al. (2018) noted that the recent decadal increase in precipitation over the Sahel  
308 is by no means a recovery to the former wet period, but rather a shift to more intermittent

309 and extreme rainfall regime. Convective clouds with extremely high tops generally produce  
310 extreme precipitation (Zhou et al., 2013; Kim et al., 2018; Klein et al., 2018). Thus, the recent  
311 increase in intense precipitation over the Sahel is likely to be related to an increase in the  
312 frequency of extreme deep convection. The most notable change in mid-summer is the  
313 increased upwelling in the TTL over the Sahel. This enhanced Sahelian upwelling may be  
314 connected with that over the Sahara, as discussed in T17, but it could also be caused by  
315 the increase in extreme deep convection penetrating to the TTL.

316

317 Increases in greenhouse gas levels have resulted in recent tropospheric warming, but the  
318 effects are not limited to the troposphere. The indirect effects generated via the enhanced  
319 Brewer–Dobson circulation and resultant ozone decrease have caused the lower tropical  
320 stratosphere to cool, which has, in turn, led to a decrease in vertical static stability in the TTL  
321 (Lin et al., 2017). The intensification of extreme deep convective activity over the Sahel in  
322 July and August in recent decades is associated with the cooling in the lower tropical  
323 stratosphere and TTL. It has been said that the effect of global warming on precipitation is  
324 that "wet gets wetter" (Held and Soden, 2006); however, in that analysis, the depth of  
325 convection was not considered. What we observe over West Africa is rather that "deep gets  
326 deeper".

327

328 It is difficult to use statistical methods to demonstrate a causality between two variables



329 exhibiting large trends, such as the vertical temperature gradient and divergence in the TTL  
330 ( $r=0.72$ ) in Fig. 7a. Over intraseasonal timescales, a causal relationship between the tropical  
331 stratospheric temperature and deep convection was demonstrated using large ensemble  
332 experiments that focused on the September 2009 SSW event (Noguchi et al., 2020). Careful  
333 inspection of their Fig. 4b over the African region reveals that precipitation over Sahel  
334 increases, while that over Guinea Coast decreases following a cooling in the TTL, similar to  
335 the present study as shown in Fig. 1b.

336

337 This model study supports a physical relationship between the temperature variation in the  
338 tropical lower stratosphere and deep convective activity that penetrates the TTL. In this study,  
339 we made use of the vertical velocity and divergence data from the JRA-55 reanalysis.  
340 However, vertical velocity is not an observable variable and depends strongly on the model  
341 (i.e., the cumulus parametrization) used for the reanalysis. This is especially true in the TTL,  
342 where there is little observational data available. Preliminary analysis of the European  
343 Centre for Medium-Range Weather Forecasts reanalysis data (ERA 5) in Western Africa is  
344 shown in supporting material (Fig. S2). There is good agreement between JRA-55 and  
345 ERA5 for air temperature at 100 hPa. Although sufficient agreement in vertical velocity is  
346 found over Guinea Coast, pressure vertical velocities at 150 hPa disagree over Sahel: no  
347 trend is detected in ERA5. Discrepancies are especially large along a zone in frequent COV.  
348 It should be noted that horizontal divergence of JRA-55 agrees quite well with a number of

349 MCS of TCC <  $-70^{\circ}$  (Figs. 7a and S1). It should also be noted that the trend in surface  
350 precipitation over the Sahel is completely missed in ERA5, while that in JARA-55 is  
351 exaggerated (Quagraine et al., 2010). This could be due to a problem of a parametrization  
352 of the cumulus convection over land in the model used for reanalysis. This is a key aspect  
353 for the understanding of the TTL role in driving deep convection in the Sahel and the Tropics,  
354 and should be investigated more in detailed in future studies.

355

356

### Acknowledgments

357 This work was supported in part by Grants-in-Aid for Scientific Research (25340010,  
358 17H01159, JP18K03743) from the Japan Society for the Promotion of Science. Preliminary  
359 analysis of this study was carried out using the Interactive Tool for Analysis of the Climate  
360 System (ITACS) provided by the Japan Meteorological Agency. AMSU data was accessed  
361 through ICARE with support of the IPSL-ESPRI team. RU was supported by NASA Upper  
362 Atmospheric Composition Observations Program.

363

364

### References

365 Adler, R.F., G.J. Huffman, A. Chang, R. Ferraro, P. Xie, J.E. Janowiak, B. Rudolf, U.  
366 Schneider, S. Curtis, D.T. Bolvin, A. Gruber, J. Susskind, P.A. Arkin, and E.J. Nelkin, 2003:  
367 The Version 2 Global Precipitation Climatology Project (GPCP) monthly precipitation  
368 analysis (1979-present). *J. Hydrometeorol.*, **4**, 1147-1167.

369 Biasutti, M., 2019: Rainfall trends in the African Sahel: Characteristics, processes, and  
370 causes. *WIREs climate change*, **10** (4), DOI: 10.1002/wcc.591.

371 Diakhaté, M., B. Rodríguez-Fonseca, I. Gómara, E. Mohino, A. L. Dieng, and A. T. Gaye, A.,  
372 2019: Oceanic forcing on interannual variability of Sahel heavy and moderate daily rainfall.  
373 *J. Hydrometeorol*, **20**, 397-410.

374 Dong, B. and R. Sutton, 2015: Dominant role of greenhouse gas forcing in the recovery of  
375 Sahel rainfall. *Nature Climate Change*, **5**, 757–760. doi: 10.1038/nclimate2664

376 Druyan, L.M., and R.D. Koster, 1989: Sources of Sahel precipitation for simulated drought  
377 and rainy seasons, *J. Clim.*, **2**, 1438 – 1446, doi:10.1175/1520-  
378 0442(1989)002<1438:SOSPFS>2.0.CO;2.

379 Eguchi, N., K. Kodera, and T. Nasuno, 2015: A global non-hydrostatic model study of a  
380 downward coupling through the tropical tropopause layer during a stratospheric sudden  
381 warming. *Atmos. Chem. Phys.*, **15**, 297–304.

382 Folland, C.K., Y.N. Palmer, and D.E. Parker, 1986: Sahel rainfall and worldwide sea  
383 temperatures 1901–85. *Nature*, **320**, 602–607. doi:10.1038/320602a0.

384 Fontaine, B., P. Roucou, M. Gaetani, and R. Marteau, 2011: Recent changes in precipitation,  
385 ITCZ convection and northern tropical circulation over North Africa (1979–2007). *Int. J.*  
386 *Climatol.*, **31**, 633–648, doi:10.1002/joc.2108.

387 Funatsu, B. M., C. Claud, P. Keckhut, A. Hauchecorne, and T. Leblanc, 2016: Regional and  
388 seasonal stratospheric temperature trends in the last decade (2002–2014) from AMSU

389 observations. *J. Geophys. Res. Atmos.*, **121**, 8172–8185,  
390 <https://doi.org/10.1002/2015JD024305>.

391 Gaetani, M., S. Janicot, M. Vrac, A.M. Famien, and B. Sultan, 2020: Robust assessment of  
392 the time of emergence of precipitation change in West Africa. *Sci. Rep.*, **10**, 7670.  
393 <https://doi.org/10.1038/s41598-020-63782-2>.

394 Giannini, A., 2010: Mechanisms of climate change in the semiarid African Sahel: The local  
395 view. *J. Climate*, **23**, 743–756, <https://doi.org/10.1175/2009JCLI3123.1>.

396 Giannini, A., S. Salack, T. Lodoun, A. Ali, A. Gaye, and O. Ndiaye, 2013: A unifying view of  
397 climate change in the Sahel linking intra-seasonal, interannual and longer time scales.  
398 *Environ. Res. Lett.*, **8**, 024010, doi:10.1088/1748-9326/8/2/024010.

399 Hart, N.C.G., R. Washington, and R.I. Maidment, 2019: Deep convection over Africa: annual  
400 cycle, ENSO and trends in the hotspots, *J. Clim.*, **32**, 8791–8811.

401 Held, I. M., and B.J. Soden, 2006: Robust responses of the hydrological cycle to global  
402 warming. *J. Clim.*, **19**, 5686–5699, <https://doi.org/10.1175/JCLI3990.1>

403 Holloway, C. E., and J.D. Neelin, 2007: The convective cold top and quasi equilibrium, *J.*  
404 *Atmos. Sci.*, **64**, 1467-1487.

405 Hong, G., G. Heygster, J. Miao, and K. Kunzi, 2005: Detection of tropical deep convective  
406 clouds from AMSU-B water vapor channels measurements, *J. Geophys. Res.*, **110**,  
407 D05205, <https://doi.org/10.1029/2004JD004949>.

408 Janicot, S., S. Trzaska, and I. Pocard, 2001: Summer Sahel-ENSO teleconnection and

409 decadal time scale SST variations. *Clim. Dyn.*, **18**, 303–320, doi:10.1007/s003820100172.

410 Kim, J., W.J. Randel, and T. Birner, 2018: Convectively driven tropopause-level cooling and  
411 its influences on stratospheric moisture. *J. Geophys. Res. Atmos.*, **123**, 590–606,  
412 <https://doi.org/10.1002/2017JD027080>.

413 Klein, C., D. Belušić, D., and C.M. Taylor, 2018: Wavelet scale analysis of mesoscale  
414 convective systems for detecting deep convection from infrared imagery. *J. Geophys. Res.*  
415 *Atmos.*, **123**, 3035–3050. <https://doi.org/10.1002/2017JD027432>.

416 Klein, C. and C. M. Taylor, 2020: Dry soils can intensify mesoscale convective systems. *Proc.*  
417 *Natl. Acad. Sci.*, **117** (35), 21132–21137.

418 Klein, C., F. Nkrumah, C. M. Taylor and E. A. Adefisan, 2020: The seasonality of drivers of  
419 storm trends in southern West Africa. *J. Clim.*, doi 10.1175/JCLI-D-20-0194.1, in press

420 Kobayashi, S., Y. Ota, Y. Harada, A. Ebita, M. Moriya, H. Onoda, K. Onogi, H. Kamahori, C.  
421 Kobayashi, H. Endo, K. Miyaoka, and K. Takahashi, 2015.: The JRA-55 Reanalysis:  
422 general specifications and basic characteristics. *J. Meteorol. Soc. Japan*, **93**, 5–48,  
423 doi:10.2151/jmsj.2015-001.

424 Kodera, K., N. Eguchi, R. Ueyama, Y. Kuroda, C. Kobayashi, B.M. Funatsu, and C. Claud,  
425 2019: Implication of tropical lower stratospheric cooling in recent trends in tropical  
426 circulation and deep convective activity. *Atmos. Chem. Phys.*, **19**, 2655-2669,  
427 doi:10.5194/acp-19-2655-2019.

428 Lin, P., D. Paynter, Y Ming, and V. Ramaswamy, 2017: Changes of the tropical tropopause

429 layer under global warming. *J. Clim.*, **30**, 1245–1258, <https://doi.org/10.1175/JCLI-D-16->  
430 0457.1.

431 Maidment, R.I., R.P. Allan, and E. Black, 2015.: Recent observed and simulated changes in  
432 precipitation over Africa. *Geophys. Res. Lett.*, **42**, 8155–8164,  
433 doi:10.1002/2015GL065765.

434 Mohino, E., S. Janicot, and J. Bader, 2011: Sahel rainfall and decadal to multi-decadal sea  
435 surface temperature variability. *Climate Dyn.*, **37**, 419–440, doi:10.1007/s00382-010-  
436 0867-2.

437 Nicholson S.E., 2013: The West African Sahel: a review of recent studies on the rainfall  
438 regime and its interannual variability. *ISRN Meteorol.*, **2013**, 1–32, doi:  
439 10.1155/2013/453521.

440 Noguchi, S., y. Kuroda, Y., K. Kodera, K., and S. Watanabe, 2020: Robust enhancement of  
441 tropical convective activity by the 2019 Antarctic sudden stratospheric warming. *Geophys.*  
442 *Res. Lett.*, **47**, e2020GL088743. doi:10.1029/2020GL088743

443 Odoulami RC, and A.A. Akinsanola, 2017: Recent assessment of West African summer  
444 monsoon daily rainfall trends. *Weather*. <https://doi.org/10.1002/wea.2965>.

445 Panthou, G., T. Vischel, and T. Lebel, 2014: Recent trends in the regime of extreme rainfall  
446 in the Central Sahel. *Int. J. Climatol.*, doi:10.1002/joc.3984.

447 Panthou, G., T. Lebel, T. Vischel, G. Quantin, Y. Sane, A. Ba, O. Ndiaye, A. Diongue-Niang,  
448 and M. Diopkane, 2018: Rainfall intensification in tropical semi-arid regions: the Sahelian

449 case. *Environ. Res. Lett.*, **13**, 064013.

450 Pu, B., and K. H. Cook, 2011: Role of the West African westerly jet in Sahel rainfall variations,  
451 *J. Clim.*, **25**, 2880–2896, doi:10.1175/JCLI-D-11-00394.1.

452 Quagraine, K.A., F. Nkrumah, C. Klein, N.A.B. Klutse, and K.T. Quagraine, 2020: West  
453 African summer monsoon precipitation variability as represented by reanalysis datasets,  
454 *Climate*, **8**, 111; doi:10.3390/cli8100111

455 Rodríguez-Fonseca B, S. Janicot, E. Mohino, T. Losada, J. Bader, C. Caminade, F. Chauvin,  
456 B. Fontaine, J. García-Serrano, S. Gervois, M. Joly, I. Polo, P. Ruti, P. Roucou, and A.  
457 Voltaire, 2011: Interannual and decadal SST-forced responses of the West African  
458 monsoon. *Atmos. Sci. Lett.*, **12**, 67 – 74, doi:10.1002/asl.308.

459 Rodríguez-Fonseca, B., E. Mohino, C.R. Mechoso, C. Caminade, M. Biasutti, M. Gaetani,  
460 J. Garcia-Serrano, E.K. Vizy, K. Cook, Y. Xue, I. Polo, Y. Losada, L. Druyan, B. Fontaine,  
461 J. Bader, F.J. Doblas-Reyes, L. Goddard, S. Janicot, A. Arribas, W. Lau, A. Colman, M.  
462 Vellinga, D.P. Rowell, F. Kucharski, and A. Voltaire, 2015: Variability and predictability of  
463 West African droughts: a review on the role of sea surface temperature anomalies. *J.*  
464 *Clim.*, **28**(10), 4034–4060, <https://doi.org/10.1175/JCLI-D-14-00130.1>

465 Rowell, D.P., 2003: The impact of Mediterranean SSTs on the Sahelian rainfall Season, *J.*  
466 *Clim.*, **16**, 849-862.

467 Rowell, D.P., 2013: Simulating SST teleconnections to Africa: what is the state of the art? *J.*  
468 *Clim.*, **26**:5397–5418. doi:10.1175/JCLI-D-12-00761.1.

469 Russo S. A.F. Marchese, J. Sillmann, and G. Immé, 2016: When will unusual heat waves  
470 become normal in a warming Africa? *Environ. Res. Lett.*, **11**, 054016,  
471 <https://doi.org/10.1088/1748-9326/11/5/054016>

472 Sultan, B. and M. Gaetani, 2016: Agriculture in West Africa in the twenty-first century:  
473 Climate change and impacts scenarios, and potential for adaptation. *Front. Plant Sci.*, **7**,  
474 1–20.

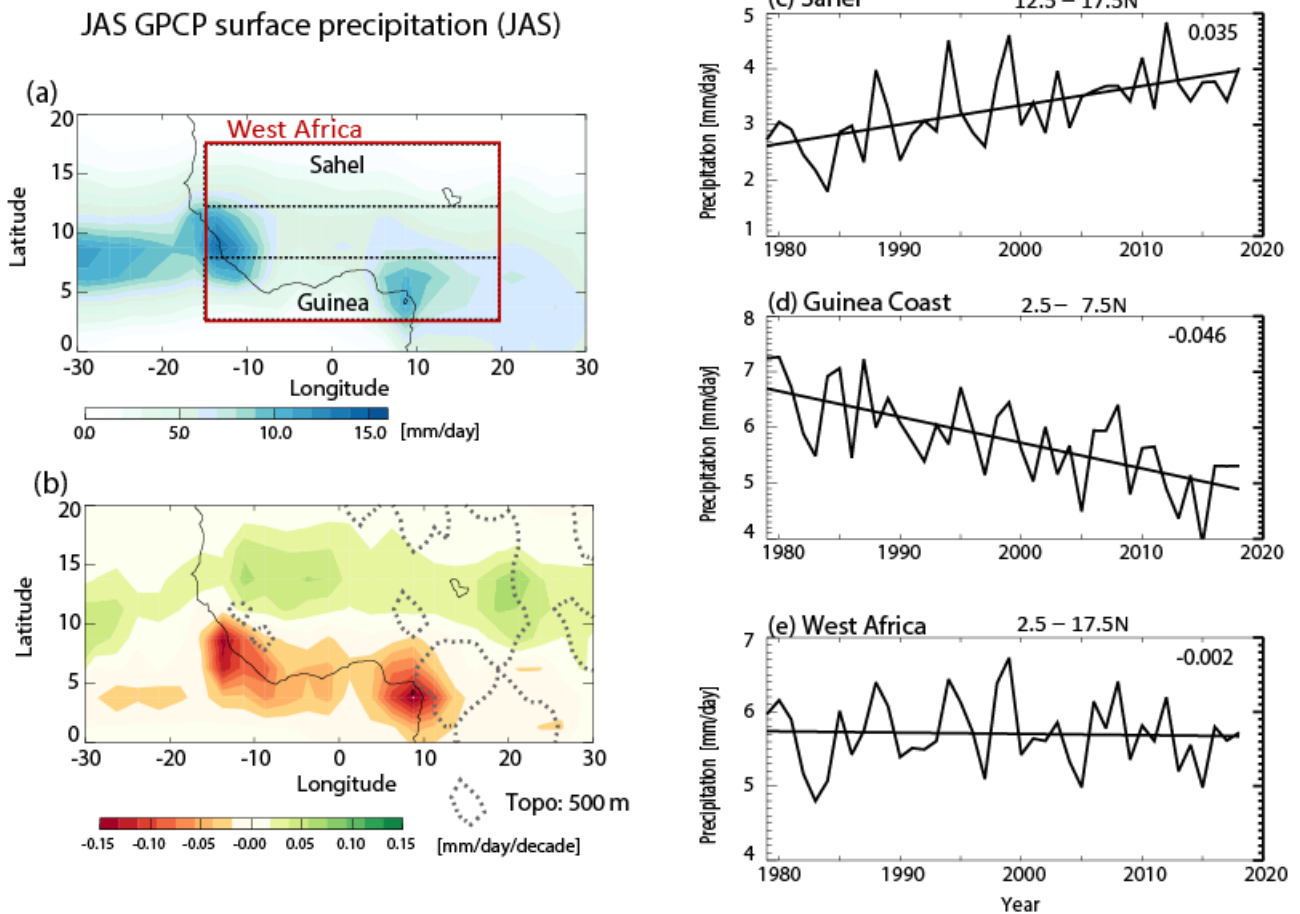
475 Taylor CM, D. Belušić, F. Guichard, D.J. Parker, T. Vischel, O. Bock, P.P. Harris, S. Janicot,  
476 C. Klein, and G. Panthou, 2017: Frequency of extreme Sahelian storms tripled since 1982  
477 in satellite observations. *Nature* **544**(7651): 475–478. doi: /10.1038/nature22069.

478 Taylor, C. M., A. H. Fink, C. Klein, D. J. Parker, F. Guichard, P. P. Harris and K. R. Knapp,  
479 2018: Earlier seasonal onset of intense mesoscale convective systems in the Congo  
480 Basin since 1999, *Geophys. Res. Lett.*, **45**(24): 13,458-413,467.

481 Zhou, Y., W.K.M. Lau, and C. Liu, 2013: Rain characteristics and large-scale environments  
482 of precipitation objects with extreme rain volumes from TRMM observations, *J. Geophys.*  
483 *Res. Atmos.*, **118**, 9673–9689, doi:10.1002/jgrd.50776

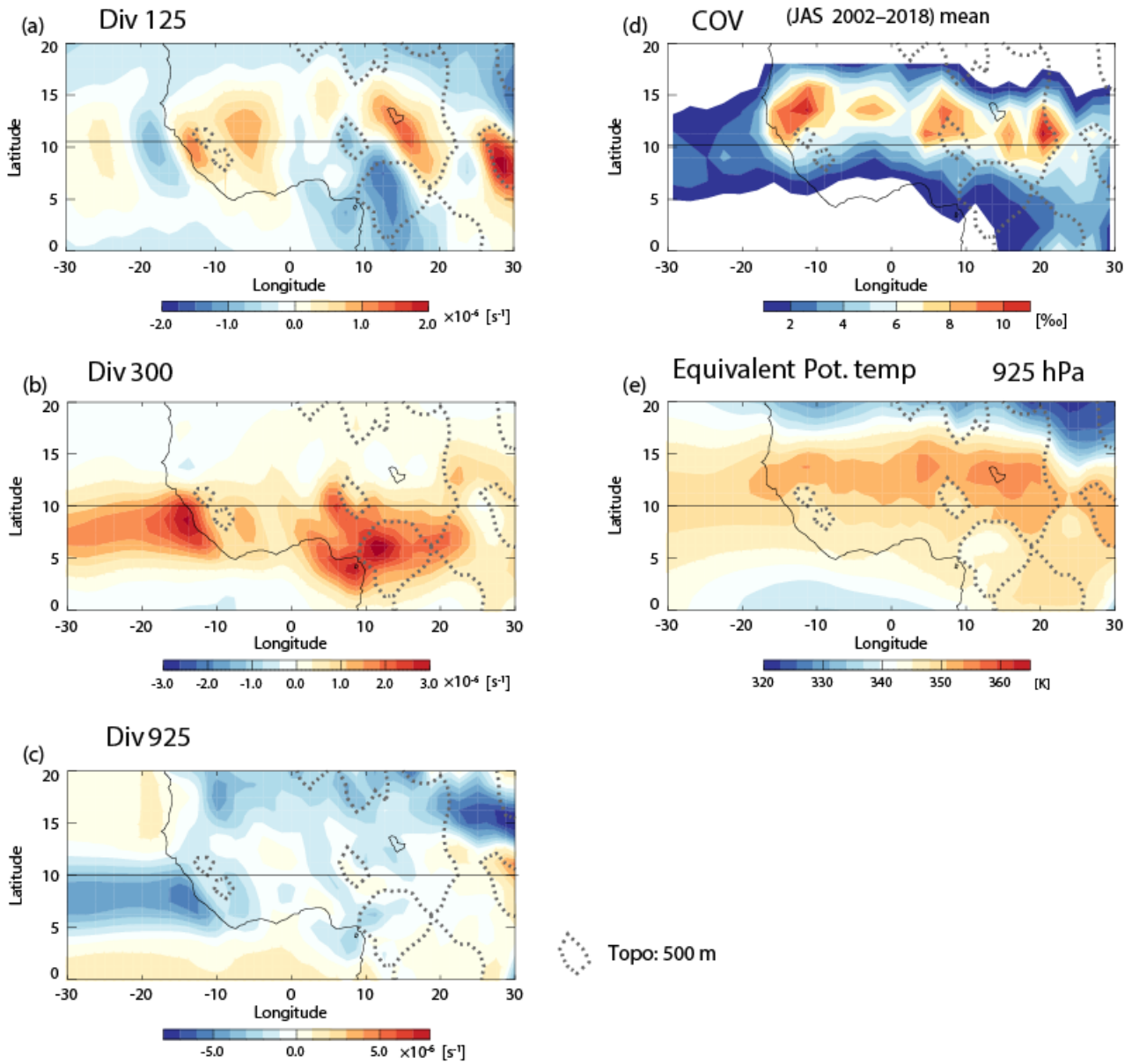
484 Zuluaga, M.D., and R.A. Houze Jr., 2015: Extreme convection of the near-equatorial  
485 Americas, Africa, and adjoining oceans as seen by TRMM., *Mon. Wea. Rev.*, **143**, 298–  
486 316, doi:10.1175/MWR-D-14-00109.1.



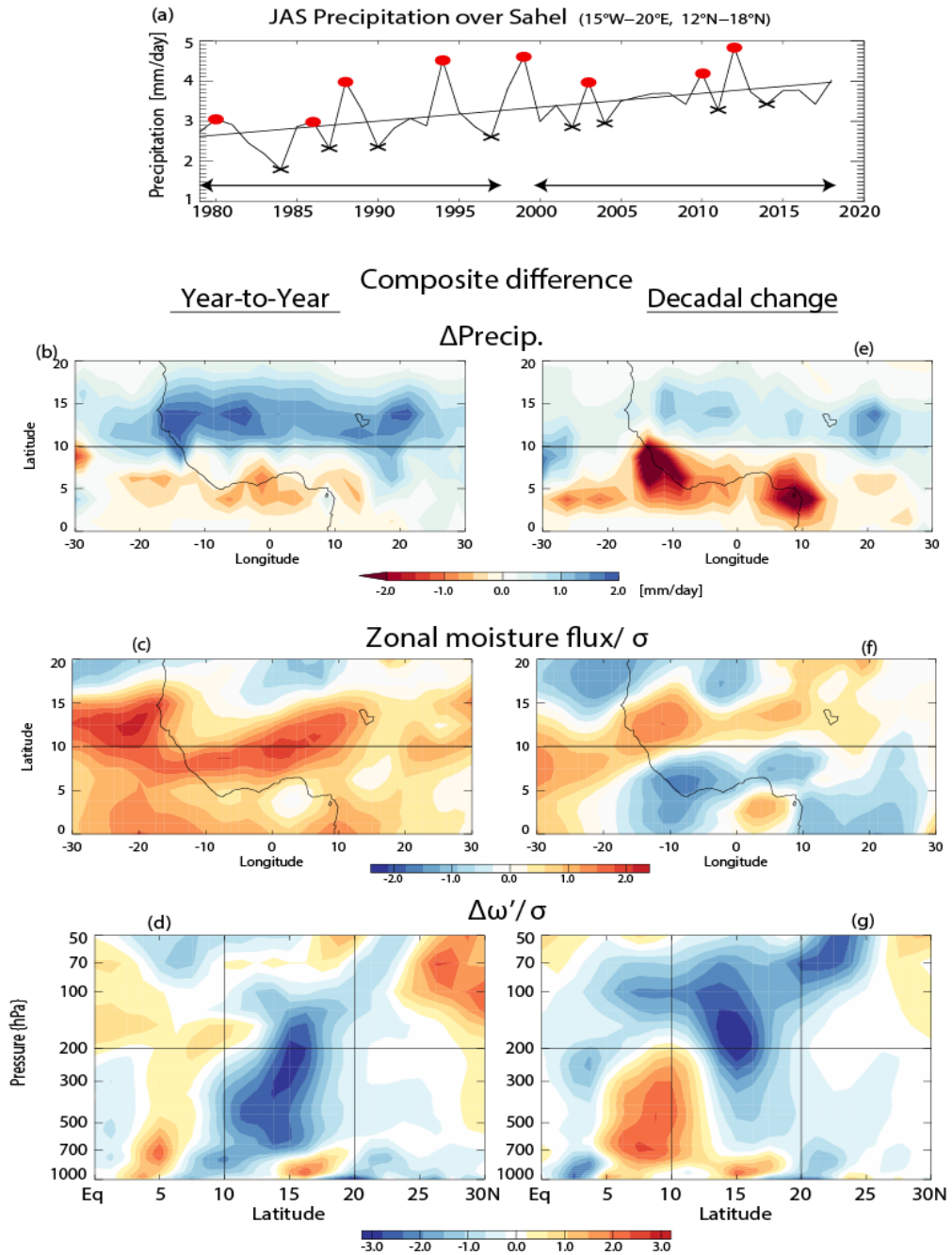


490 Fig. 1 (a) Climatological mean surface precipitation over West Africa during JAS and (b) its  
 491 linear trend over the period 1979–2018. (c, d, and e) Time series of JAS mean  
 492 precipitation averaged over (c) the Sahel, (d) the Guinea Coast, and (e) West Africa.  
 493 Straight lines and numbers indicate linear trend (mm/day/decade). Regions within West  
 494 Africa are indicated by dotted lines within the brown box in (a). Contours with dotted lines  
 495 indicate topography of 500 m.

## JAS Climatology (1979–2018)



496 Fig. 2 Climatology for JAS. Horizontal divergence at (a) 125, (b) 300, and (c) 925 hPa. (d)  
 497 Frequency of convective overshooting. (e) Equivalent potential temperature at 925 hPa.  
 498 Contours with dotted lines indicate topography of 500 m.



499

500

501

Fig. 3 (a) Time series of JAS mean surface precipitation over the Sahel from GPCP. Red

502

dots and black crosses indicate wet and dry summers, respectively. (b–d) Composite

503

mean differences between wet and dry summers: (b) surface precipitation, (c)

504

standardized anomalous zonal moisture flux at 850 hPa, and (d) standardized anomalous

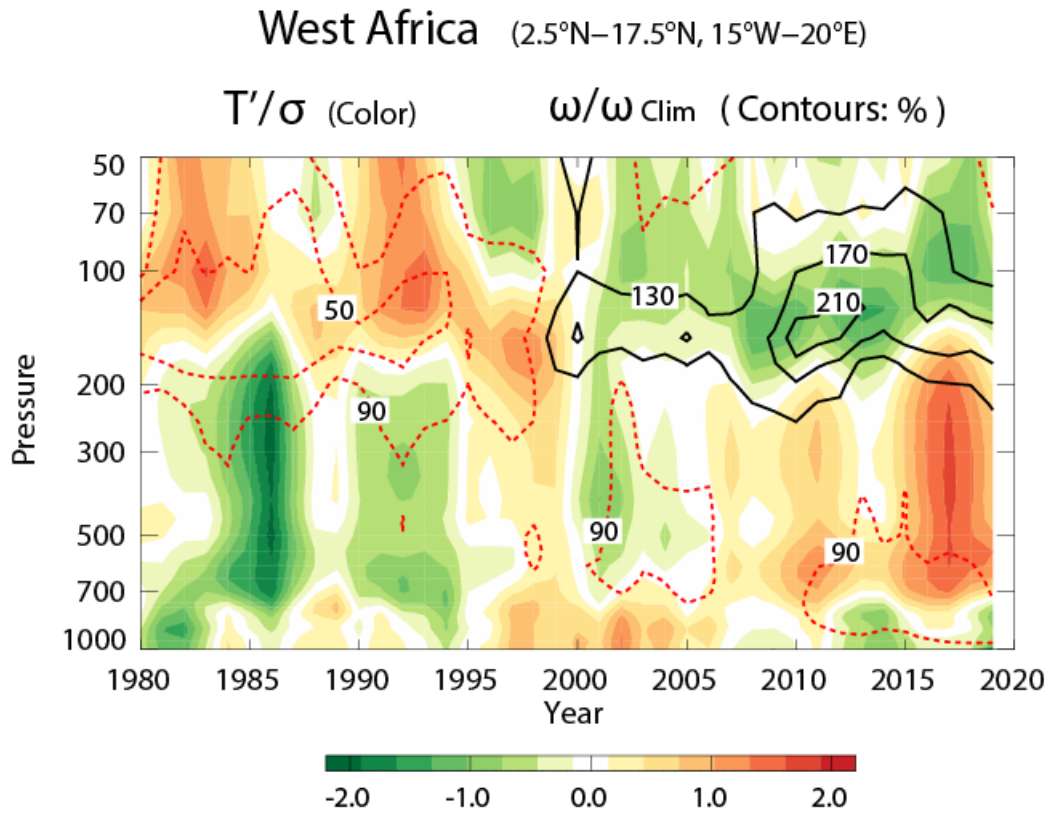
505

pressure vertical velocity over the West African sector (15°W–20°E). (e, f, g) As (b, c, d)

506

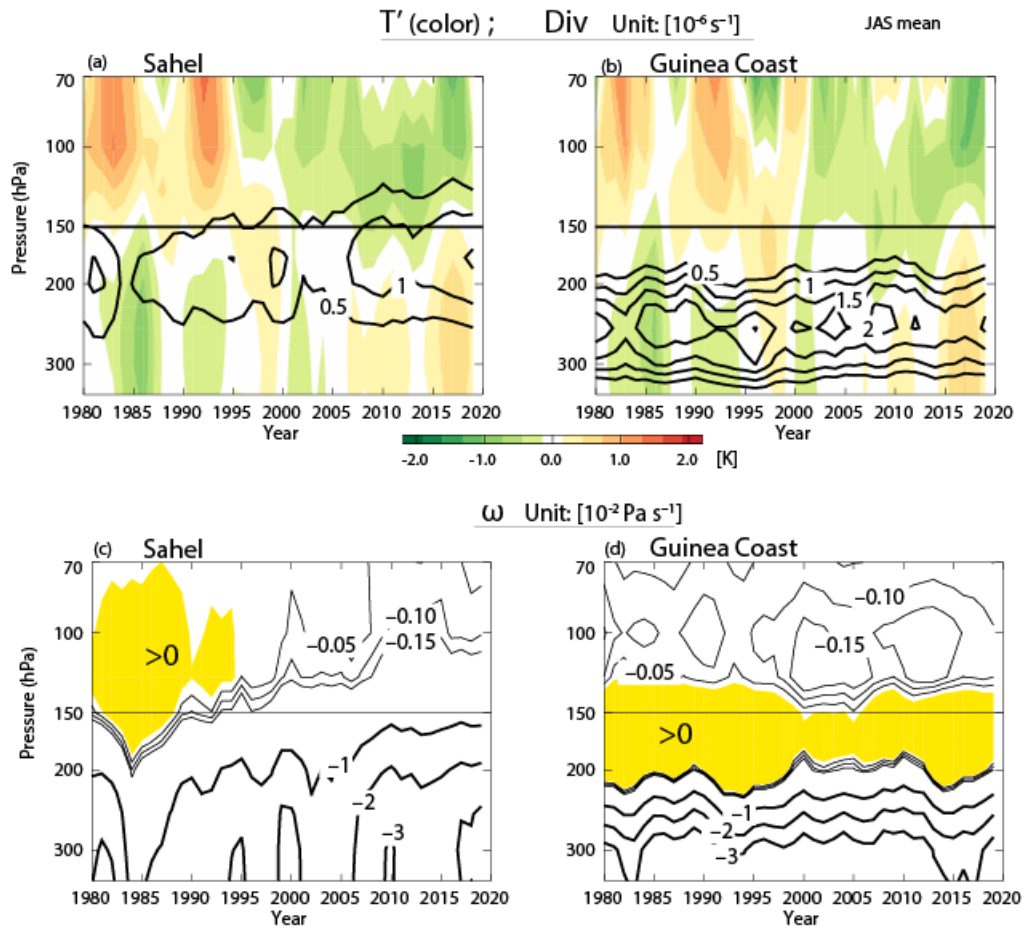
except the differences were calculated between two 19-year periods; 2000–2018 and

507 1979–1997 indicated by two arrows in (a).



508

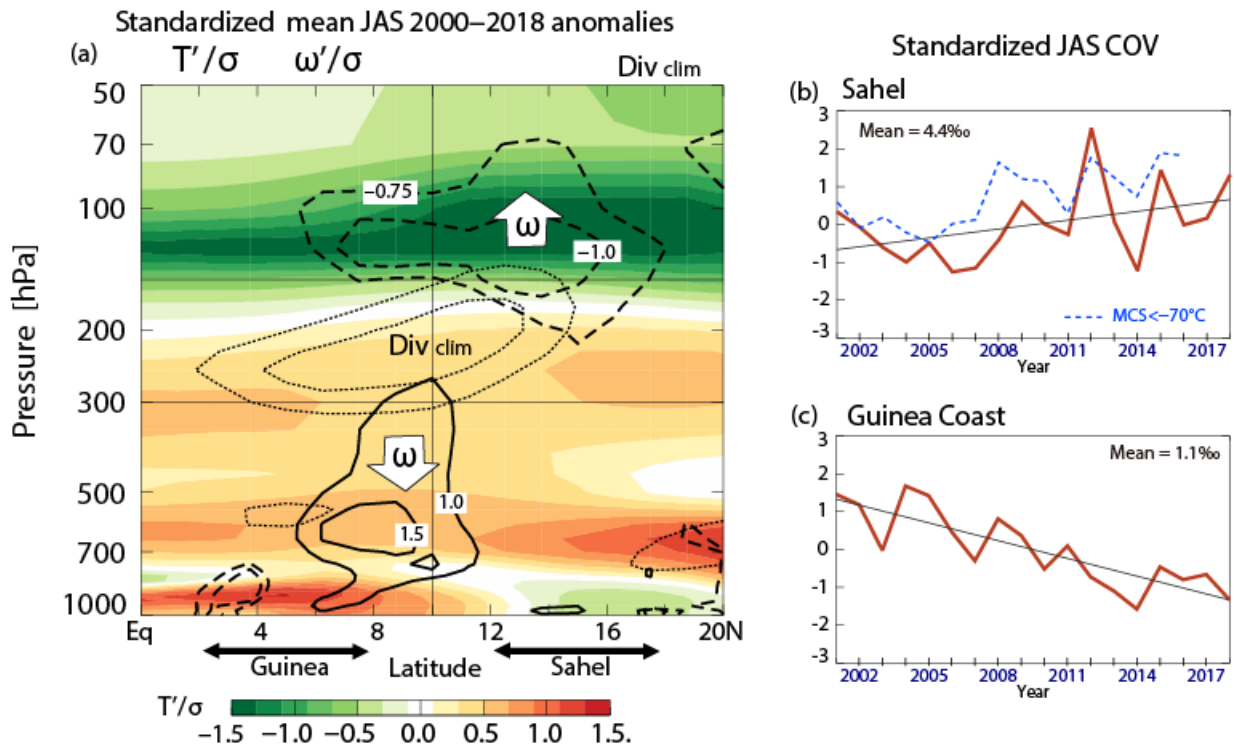
509 Fig. 4 Height–time cross-section over West Africa of JAS mean standardized anomalous  
510 temperature (color shading) and amplitude (%) of pressure vertical velocity relative to its  
511 climatological value (contours: 100% > by black lines, and < 100% by red dashed lines).  
512 A 3-year running mean has been applied to the data.



513

514 Fig. 5 JAS mean (a, b) horizontal divergence (contours) and anomalous temperature (color  
 515 shading) and (c, d) pressure vertical velocity ( $\omega$ ) (contours). Yellow shading indicates the  
 516 region of downward velocity. Left- and right-hand panels are for the Sahel ( $12.5^{\circ}$ – $17.5^{\circ}$ N )  
 517 and Guinea Coast ( $2.5^{\circ}$ – $7.5^{\circ}$ N), respectively. A 3-year running mean has been applied to  
 518 the data.

519

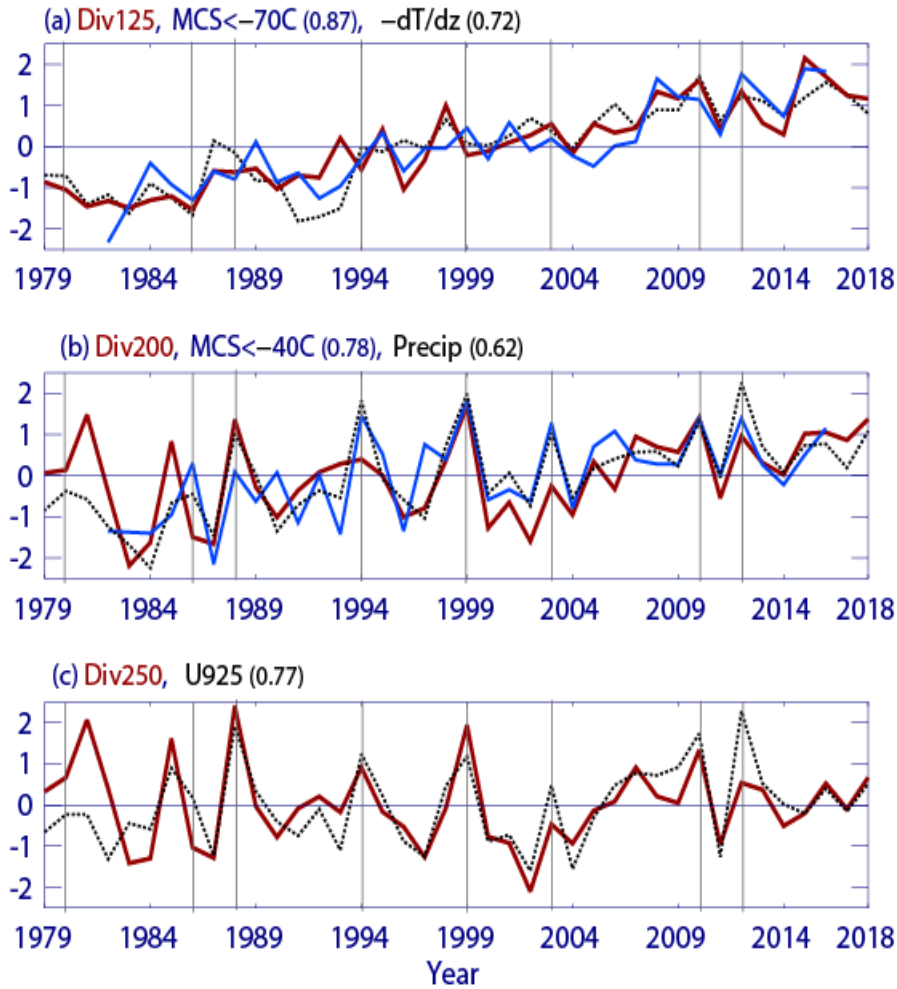


520

521 Fig. 6 (a) Meridional cross-section of standardized mean JAS 2000–2018 anomalies over  
 522 the West African sector (15°W–20°E). Temperature is shown by color shading, and  
 523 pressure vertical velocity are shown by contour lines (positive by solid lines, and negative  
 524 by dashed lines). Climatology of the horizontal divergence is shown by dotted lines.  
 525 Contours are for 1, and 2  $\times 10^{-6}$  s $^{-1}$ . (b, c) Standardized JAS mean COV occurrence  
 526 frequency from 2001 to 2018 over (b) the Sahel and (c) the Guinea Coast. These two  
 527 regions are indicated by the arrows along the x-axis of (a). Blue dashed lines in (b) indicate  
 528 the standardized JAS mean MCSs with a CTT below  $-70^{\circ}\text{C}$  from T17 (same as in Fig.  
 529 7a).

530

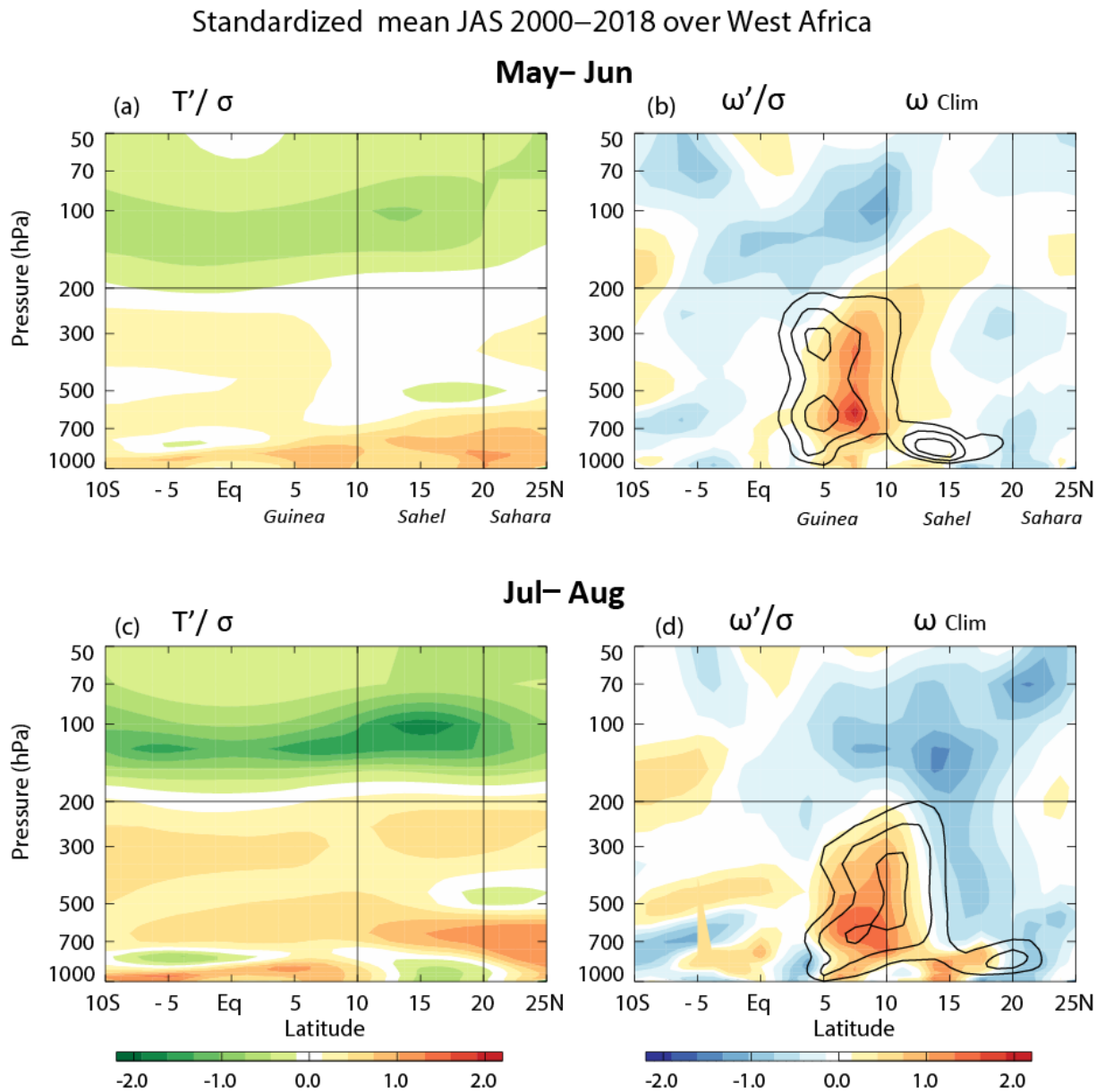
### JAS mean standardized anomalies over Sahel



531

532 Fig. 7 Time series of JAS mean standardized anomalies. (a) Horizontal divergence at 125  
 533 hPa (brown lines), occurrence frequency of MCSs with a CTT below  $-70^{\circ}\text{C}$  (blue lines),  
 534 and anomalous temperature differences between 125 and 175 hPa (black dotted lines).  
 535 (b) Horizontal divergence at 200 hPa (brown lines), MCSs with a CTT below  $-40^{\circ}\text{C}$  (blue  
 536 lines), and surface precipitation (black dotted lines). (c) Horizontal divergence at 250 hPa  
 537 (brown lines) and anomalous zonal wind over the Atlantic Ocean ( $10^{\circ}\text{N}$ – $15^{\circ}\text{N}$ ,  $30^{\circ}\text{W}$ –  
 538  $15^{\circ}\text{W}$ ) at 925 hPa (black dotted lines). The correlation coefficients between the divergence  
 539 and other variables are indicated on the top of each panel. Vertical lines indicate peak  
 540 years in the year-to-year variability of surface precipitation in Fig. 3a.

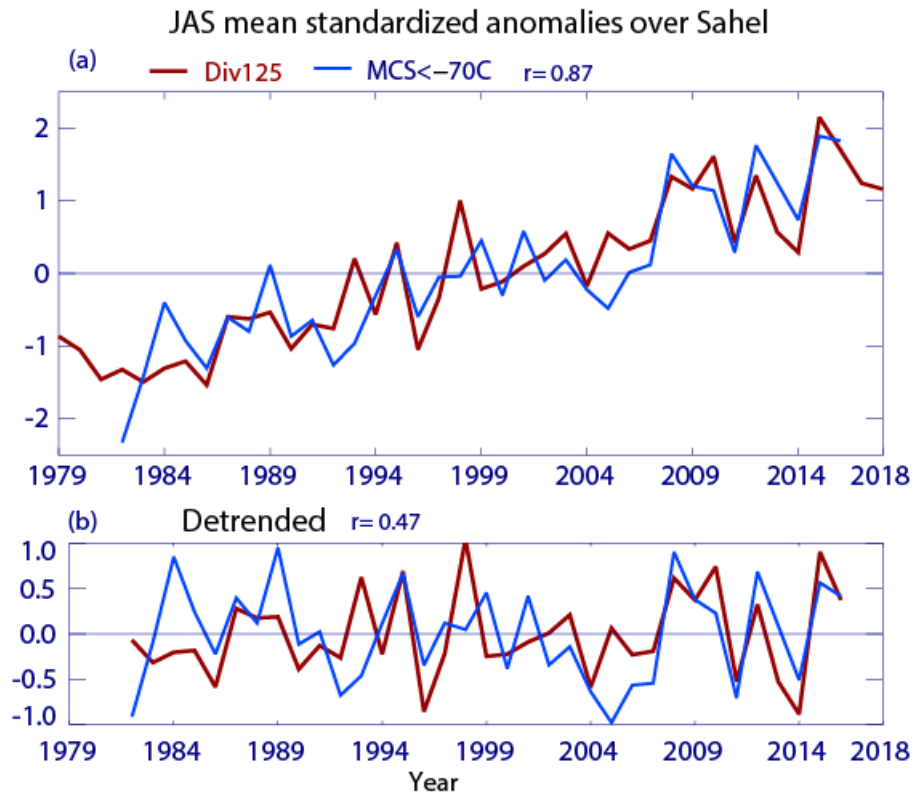
541





549 **Supporting Figures**

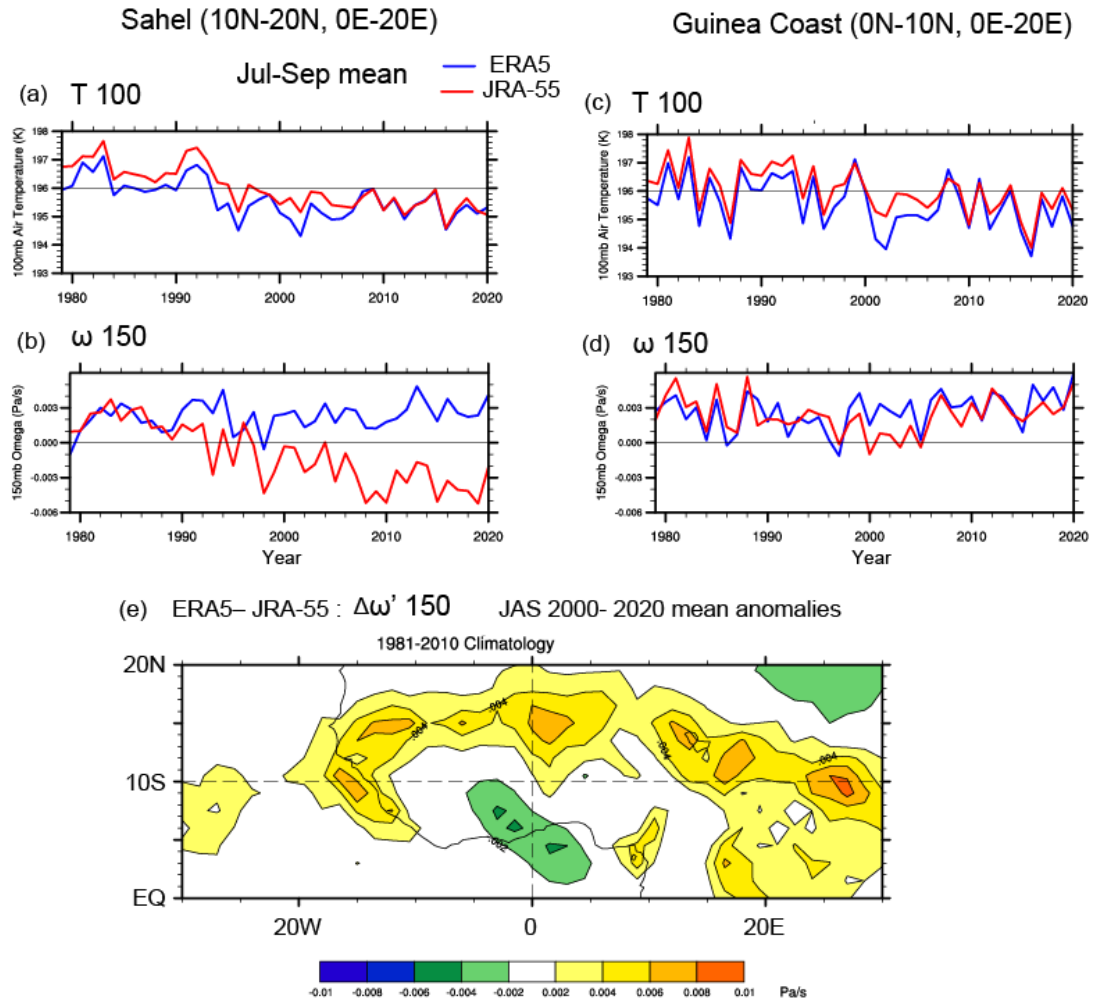
550



551 Fig. S1 (a) Time series of JAS mean standardized anomalies for horizontal divergence at  
552 125 hPa (brown lines), occurrence frequency of MCSs with CTT below  $-70^{\circ}\text{C}$  (blue lines)  
553 same as in Fig. 7a. (b) Same as (a), but for the detrended time series. Correlation  
554 coefficients between the two variables are 0.87 for (a) and 0.47 for (b) based on the 35-  
555 year data.

556

557



558 Fig. S2 Comparison between JRA-55 and ERA5 reanalyses. (a) JAS mean air temperature  
 559 at 100 hPa over Sahel (10°N–20°N, 0°E–20°E) from 1979 to 2020. Red and blue lines are  
 560 for ERA5 and JRA-55 reanalyses, respectively. (b) Same as in (a), except for pressure  
 561 vertical velocity at 150 hPa ( $\omega_{150}$ ). (c and d) Same as (a and b) except for over Guinea  
 562 Coast (0°N–10°N, 0°E–20°E). Equatorial temperature variation related with the  
 563 stratospheric QBO is visible in (c). (e) Difference in spatial structure of seasonal difference  
 564 in anomalous  $\omega_{150}$  from climatology between ERA5 and JRA-55 during recent decades  
 565 (JAS 2000–2020 mean). Difference is large where extreme deep convection is frequent  
 566 (*c.f.* Fig. 2). Climatology is JAS 1981–2010. Images are provided by the NOAA-ESRL  
 567 Physical Sciences Laboratory, Boulder Colorado from their Web site at  
 568 <https://psl.noaa.gov/>.